sustainability

MDPI

Article

Pre-Solve Methodologies for Short-Run Identification of Critical Sectors in the ACSR Overhead Lines While Using Dynamic Line Rating Models for Resource Sustainability

Hugo Algarvio

LNEG-National Laboratory of Energy and Geology, Est. Paço do Lumiar 22, 1600-038 Lisbon, Portugal; hugo.algarvio@tecnico.ulisboa.pt

Abstract: Most transmission system operators (TSOs) use seasonally static models considering extreme weather conditions, serving as a reference for computing the transmission capacity of power lines. The use of dynamic line rating (DLR) models can avoid the construction of new lines, market splitting, false congestions and the degradation of lines in a cost-effective way. The operation of power systems is planned based on market results, which consider transactions hours ahead of real-time operation using forecasts with errors. The same is true for the DLR. So, during real-time operation TSOs should rapidly compute the DLR of overhead lines to avoid considering an ampacity above their lines' design, reflecting the real-time weather conditions. Considering that the DLR of the lines can affect the power flow of an entire region, the use of the complete indirect DLR methodology has a high computation burden for all sectors and lines in a region. So, this article presents and tests three pre-solve methodologies able to rapidly identify the critical sector of each line. These methodologies solve the problem of the high computation burden of the CIGRÉ thermodynamic model of overhead lines. They have been tested by using real data of the transmission grid and the weather conditions for two different regions in Portugal, leading to errors in the computation of the DLR lower than 1% in relation to the complete CIGRÉ model, identifying the critical sector in significantly less time.

Keywords: ampacity; dynamic line rating; pre-solve methodology; real-time operation; transmission system operators; weather conditions

Academic Editor: Mokhtar Aly

Received: 10 March 2025
Revised: 9 April 2025
Accepted: 16 April 2025
Published: 21 April 2025

Citation: Algarvio, H. Pre-Solve Methodologies for Short-Run Identification of Critical Sectors in the ACSR Overhead Lines While Using Dynamic Line Rating Models for Resource Sustainability. *Sustainability* **2025**, *17*, 3758. https://doi.org/10.3390/su17083758

1. Introduction

Traditionally, most transmission system operators (TSOs) use a "steady-state" thermal equilibrium model using reference extreme weather conditions to design the maximum seasonal ampacity allowed per line, known as the seasonal line rating (SLR) [1,2]. They use reference values for the wind speed between 0.5 and 0.61 m/s and for the irradiance between 1000 and 1150 W/m^2. Normally the reference value of the air temperature is adjusted seasonally, and the wind direction is neglected. These reference values are different from the ones used by the conductors' manufacturers in their tests, performed to define the limit ampacities of the conductors [3,4].

The European Union is increasing the investment in renewable energy sources (RESs) to comply with the 2030 goals. It also aims to harmonize prices in the internal market of electricity. So, there is a need to reinforce the national and cross-border transmission capacity of the grid [5,6]. Current static models usually underestimate the real transmission capacity of overhead lines. So, using numerical indirect dynamic line rating (DLR) models such as IEEE 738-2023 [7], Kuipers and Brown [8] and CIGRÉ [9] could avoid

the construction of new lines. The use of indirect DLR models can be important in the long run by avoiding the construction of new lines but also in the short run by avoiding market splitting, "virtual" false congestions, RES curtailments and the degradation of the lines [1,2,10,11]. Several studies indicate that, on average, DLR allows for increasing the capacity of SLR from 10% to 30%, identifying that the line capacity is underestimated around 80% of the time, when the increased capacity could avoid "virtual" congestions and unnecessary RES curtailments [1,3,12–16]. When the line capacity is overestimated the use of DLR is also important to guarantee the security of the power system, avoiding the degradation of the lines such as line outages [16–18]. Past studies indicated that the line is always cooled, and with a wind speed never below 0.6 m/s, considering a natural convection, those studies were used to define the SLR used today [19–21]. A recent study of the International Electrotechnical Commission also indicated that the forced convection [22] should be always used. However, the DLR models refute those studies using experiments considering low or no wind speeds [7–9] and identify several real-world cases where the wind speed is below 0.6 m/s. So, in some hours TSOs might be operating their lines over their thermal limits [12,13,18,23].

Electricity markets are divided into wholesale and retail markets [24]. In the wholesale market, producers can submit bids to the markets or privately negotiate bilateral contracts with retailers or big consumers. In the retail market, retailers and consumers negotiate private bilateral contracts. Then retailers acquire the energy that their consumers require from wholesale markets [25]. Electricity markets are composed of long-term bilateral contracts and two spot markets based on auctions, the day-ahead market and the intraday market (in Europe, while it is the real-time market in the USA and Australia) [26]. This last market allows trades close to real-time operation where players can cover their short-run deviations from agreements settled in the long- to medium-term markets [27]. Spot markets are cleared using the marginal pricing theory, which has the goal of increasing the general welfare of the participants [28]. TSOs must evaluate the feasibility of the deals to avoid congestion and guarantee the security of the power system. So, when planning the power flow of such deals they use the fixed "steady-state" maximum ampacity of the lines, making infeasible some of the bids, increasing market prices, and reducing the general welfare of the participants [29]. In coupled regions, TSOs manage cases of market splitting using an SLR of the tie-lines' transmission capacity for the interconnection exchange between regions. They also manage the balancing markets by computing the hourly secondary reserve requirements and the secondary and tertiary reserves' real-time settlement, considering the seasonal line limits and the real-time imbalance between supply and demand [30,31].

Variable renewable energy sources (vRESs) and players from the demand-side use forecasts to predict their production and consumption, respectively. Those forecasts are subject to errors, originating deviations concerning the planning during real-time operations that must be fixed in the balancing markets [31–34]. With the increasing levels of vRESs in the power system, the planning of TSOs using seasonal models is not viable, because they are constraining the transmission grid while computing power flows considering consumption and production with significant errors. So, "virtual" false congestions can be obtained, not accepting such transactions based on power flows computed using data with errors [16,17,31–34]. Thus, TSOs should increase the efficiency of their operation by considering DLR models. In the medium term, DLR models also use weather forecasts. So, they use meteorological data with errors that should be fixed closer to real-time operation [10,16,35,36]. The problem is that DLR models have a high computational burden, being not viable to be used in large transmission grids closer to real-time operation.

Against this background, the goal of this article consists of presenting pre-solve methodologies that can rapidly identify the critical sector of each transmission line by using the effect of the weather sensitivity variables on the DLR. The critical sector of the line is the sector that minimizes the line ampacity considering the dynamic weather conditions [13,31]. All sectors affect the thermodynamic model of the line, but defining the critical sector of the line implies the DLR is an approach that mitigates the risk of using weather forecasts [37–40]. The pre-solve methodologies use a regression analysis tested in five different overhead aluminum conductor steel reinforced (ACSR) conductors of two regions of Portugal with different weather conditions [31]. While region A has a high potential for wind power with more unstable weather conditions, region B has a high potential for solar power, being the warmest region of Portugal [8,13,38]. After the identification of the critical sector, the DLR model computes the maximum ampacity of the line. As in the literature, this study ignored the distribution of the radial and axial conductor temperature such as the evaporative and corona cooling effect on the conductor [9,18,39].

Section 2 presents a literature review of the influence of weather-sensitive variables on DLR. Section 3 presents the thermodynamic model to compute the DLR of overhead lines. Section 4 presents an analysis of the effect of weather-sensitive variables on the DLR of the lines. Section 5 presents pre-solve methodologies to rapidly compute critical sectors of overhead lines. Section 6 identifies the case study and describes the data used in this work. Finally, Section 7 presents some concluding remarks.

2. Review of the Influence of Weather-Sensitive Variables on DLR

A complete review of DLR forecasting is presented in [40]. An overview of recent DLR applications and their studies and outputs is presented in [41].

Teng et al. [16] extended a two-stage stochastic optimization model with a probabilistic forecast of a DLR methodology to a model that considers the uncertainty associated with wind production, line ratings and line outages. This piece of work has the goal of co-optimizing generation and reserve holding levels in the programming phase, computing the power flow such as the re-dispatch decisions during real-time operation. The authors concluded that the use of DLR increases the utilization of the line capacity but also the reserve holding and utilization, but its cost–benefit ratio is positive.

Pavlinic and Komen [23] used a regression analysis to compute the effect of the weather-sensitive variables over the steady-state line ampacity. In their case study, they used three different regions and conductors of the Croatian transmission grid. The regression performed for conductors of each region led to errors between 0.08% and 2.26% compared with the steady-state values and depending on the region–conductor pair. They also performed a regression using three conductors, the error standing between 1.2% and 3.2% depending on the region.

In the presented work a similar approach is applied to the DLR computation and using only one regression analysis for all regions and conductors, facilitating its replicability. A sensitivity analysis of the DLR was performed in several studies but without considering the weather-sensitive variables [1,7–9,37].

Li et al. [33] used a methodology to verify the impacts of the weather-sensitive variables (wind speed and direction, ambient temperature and irradiance) on the distributed solar PV accommodation evaluation, which includes the temperature-dependent resistance and the DLR of the conductors. The results indicated that, by applying the DLR, the PV production increases by 2.59% and the economic benefit of the investors increases by 5.05%.

Dupin et al. [35] evaluated four different machine learning algorithms to compute the day-ahead DLR forecasts and compared them with the SLR approach. They considered quantile regression forest (QRF) the more reliable algorithm, increasing the line rating by

35% on average. Dupin et al. [36] upgraded the previous paper by considering the risk aversion of the TSO when deciding to accept or penalize high-risk situations. The authors defined the value of EUR 1500 as the limit cost in the use of the reserve because of the DLR forecasting errors, computing the frequency of occurrence of these incidents, with the TSO being responsible for them. The forecasting errors have a mean absolute percentage error (MAPE) of 11.1% and 16.1% for the QRF and for the persistence algorithms, respectively. When the TSO used a risk-neutral strategy it obtained a benefit of 1% concerning the SLR and a frequency of occurrence of incidents around 1.1%, while considering a perfect forecast strategy it had a benefit of 1.1%.

Viafora et al. [34] proposed a DC-optimal power flow algorithm that considers the DLR and the wind uncertainty considering the typical risk aversion in the line rating forecast. They used a case study in which they compared the costs with day-ahead dispatch, upward and downward reserves and wind curtailments. All costs decreased except for the downward reserve cost because of the extra line capacity required in the DLR model. The cost of wind curtailments decreased by 55% and the total costs decreased by 18%.

3. Thermodynamic Model to Compute the DLR of Overhead Lines

During real-time operation, TSOs may employ direct DLR methodologies, such as measuring line temperatures, to detect congestion and prevent outages [41]. However, power system operations are planned well in advance, beginning at least a day ahead, following the clearing of the day-ahead market and subsequent intraday markets [6]. In this process, the market operator provides the system operator with the optimal (cleared) market participant schedules. The system operator then simulates power flows for the programmed dispatch using an SLR approach on both internal and tie-lines. This simulation incorporates the energy outputs from the market alongside pre-existing commitments, such as long-term bilateral agreements. However, the SLR approach may identify "virtual" congestion, leading to the removal or limitation of more competitive bids in electricity markets. The interaction between market and system operators is finalized once congestion and other grid issues are extinguished. At this point, the market operator determines the clearing prices, while the TSO establishes the programmed dispatches. To prevent the exclusion of more competitive bids from electricity markets, an indirect DLR approach should be employed to determine line capacities. One such approach is the CIGRÉ thermodynamic model for overhead lines, used in this study [9,42]. This model incorporates weather forecasts to enhance grid capacity calculations [40]. In this model the thermal inertia of the conductor of an overhead conductor is calculated as the balance of gained and lost heat considering the equilibrium situation where the body does not have internal energy [7,9,42]:

$$Pc - Pr + Ps + Pj = 0 \quad (1)$$

where Pc is the convective cooling, Pr is the radiative cooling, Ps is the solar heating and Pj is the joule heating (W/m).

The active power, P (MW), of the alternating current (AC) circuit is obtained through the most common formulation as [9,42]:

$$P = U \times I_{AC} = R_{AC} \times {I_{AC}}^2 = R_{DC} \times {I_{DC}}^2 \quad (2)$$

where U (V) is the conductor voltage, I_{AC} (A) is the AC current and R_{AC} (Ω) is the AC resistance of the conductor. For a conductor with an ace core, the heating effect of the conductor is based on the equality between the alternating and the continuous (DC) power at the entrance of the conductor for the same average temperature in the conductor [9,42]. I_{DC} is the direct current of the conductor and R_{DC} the DC resistance. As the conductors'

fabricants only gave the experimental values for the R_{DC} at 20 °C, R_{DC20}, being the joule heating gain per unit length for conductors, is obtained from [9,43]:

$$Pj = {I_{DC}}^2 \times \frac{R_{DC20}}{{N_{cables}}^2} \times \left(1 + \alpha \times \left(T_{sup} - (20^\circ + Kelvin)\right)\right) \quad (3)$$

where N_{cables} is the number of conductors per line, α is the temperature coefficient per electrical resistance (1/°K), T_{sup} is the conductor temperature (°K) and $20 + Kelvin$ is the reference (20 °C) temperature (in °K), with $Kelvin$ being a conversion factor equal to 274.15. The solar heating per unit length is estimated by the standard as [9,43]:

$$Ps = alpha \times Irr \times D_{cable} \quad (4)$$

where $alpha$ is the solar absorptance (unidimensional), Irr is the solar irradiance per square meter (W/m^2) and D_{cable} is the conductor diameter (m).

Applying the Stefan–Boltzmann law, the heat loss from the conductor due to radiation, the radiative cooling, can be expressed as [9,42–44]:

$$Pr = \pi \times D_{cable} \times \sigma_b \times \varepsilon \times \left({T_{sup}}^4 - {T_a}^4\right) \quad (5)$$

where σ_b is the Stefan–Boltzmann constant (kg s^{-3} K^{-4}), ε is the conductor emissivity (unidimensional) and T_a is the ambient temperature (°K).

The convective heat loss can be expressed as a function of the dimensionless Nusselt number, Nu, as follows [9,42,43]:

$$Pc = \pi \times \lambda_f \times Nu \times \left(T_{sup} - T_a\right) \quad (6)$$

where λ_f is the thermal conductivity of air (W/mK). When the wind speed, v, is lower than 0.1 m/s it is considered the case of natural convection, computing the Nusselt number of the natural convection Nu_{NC}, as follows [9,42,43]:

$$Nu = Nu_{NC} = A_2 \times (Gr \times Pra)^{m_2} \quad (7)$$

where A_2 and m_2 are experimental parameters that depend on the multiplication value of the Grashof number, Gr, with the Prandtl number, Pra. The Grashof number approaches the proportion of the buoyancy to viscous force acting on a fluid and can be expressed as [9,42]:

$$Gr = \left[{D_{cable}}^3 \times g \times (T_{max} - T_a)\right] / \left[T_f \times {\vartheta_f}^2\right] \quad (8)$$

where g (m^2/s) is the gravity acceleration, T_{max} (°K) is the maximum static temperature supported by the conductor, T_f (°K) is the adjacent temperature to the conductor, ϑ_f (m^2/s) is the kinematic viscosity of air, computed with the dynamic viscosity of the air, μ_f, fixed to y, and the air density at a given altitude, h_a, taking into account the air density at sea level [9,43]:

$$T_f = \frac{(T_{max} + T_a)}{2} \quad (9)$$

$$\mu_f = 0.17 \times 10^{-6} + 4.635 \times 10^{-8} \times T_f - 2.03 \times 10^{-11} \times {T_f}^2 \quad (10)$$

$$y = \frac{1.293 - 1.525 \times 10^{-4}\, h_a + 6.379 \times 10^{-9}\, {h_a}^2}{1 + 0.00367 \times T_f} \quad (11)$$

$$\vartheta_f = \mu_f / y \quad (12)$$

The Prandtl number, *Pra*, approaches the proportion of kinematic viscosity to thermal diffusivity and can be expressed as [9,43]:

$$\text{Pra} = Cp_{air} \times \mu_f / \lambda_f = 0.715 - 2.5 \times 10^{-5} \times T_f \quad (13)$$

where λ_f (W/mK) is the heat conductivity of the air.

When the wind speed is higher than 0.5 m/s it is considered forced convection, and the Nusselt number is computed as [9,42]:

$$Nu = Nu_{FC} = Nu_{90} \times (A_1 + B_2 sin(\delta)^{m_1}) \quad (14)$$

$$Nu_{90} = B_1 \times Re^n \quad (15)$$

$$\delta = \theta - \xi \quad (16)$$

where Nu_{90} is the Nusselt number for an incident angle in the conductor, δ (rad), of 90° ($\pi/2$), θ is the wind direction and ξ is the conductor orientation in relation to the east reference. A_1, B_2 and m_1 are experimental parameters that depend on the incident angle. B_1 and n are experimental values that depend on the conductor roughness and on the Reynolds value, *Re*, used to forecast flow patterns in several fluid flow scenarios, and it is computed as follows [9,43]:

$$Re = v \times D_{cable} / \vartheta_f \quad (17)$$

Considering the CIGRÉ report, for wind speeds up to 0.5 m/s the incident angle of the forced convections is fixed at 45°, with the Nusselt number being [9]:

$$Nu = Nu_{45} \quad (18)$$

For wind speeds between 0.1 and 0.5 m/s it is considered that the convective power could be natural or forced, so the Nusselt number is computed as the maximum between them:

$$Nu = max(Nu_{NC}, Nu_{45}) \quad (19)$$

Considering Equations (1)–(3), the dynamic AC ampacity can be computed as [9,45]:

$$I_{DC} = \sqrt{(-Pc - Pr + Ps + Pj) / [R_{DC20} * (1 + \alpha * (T_{sup} - (20^\circ + Kelvin)))]} \quad (20)$$

$$I_{AC} = I_{DC} * N_{cables} / \sqrt{2.36\ 10^{-5} * I_{DC} * k_j} \quad (21)$$

$$k_j = R_{AC} / R_{DC} = 1.0123 \quad (22)$$

Then the apparent power limit of the transmission line, *S* (VA), is computed as:

$$S = I_{AC} * U * \sqrt{3} \quad (23)$$

4. Effect of the Weather Conditions over the Conductors' DLR

From the CIGRÉ thermodynamic model it is possible to verify that the wind speed, the wind incident angle, the ambient temperature and the irradiance are the weather sensitivity variables that affect the DLR computation [9,42]. The influence of these variables is identified and tested in this section for reference high-tension conductors.

Table 1 identifies the reference conductors and their nominal ampacity computed during the manufacturers' experimental tests using reference values for the weather variables. Using the thermodynamic formulation presented in Section 2, various scenarios were simulated by altering weather sensitivity variables. The objective was to analyze the

impact of these changes on the equilibrium relationship for the reference conductors, as defined in Equation (1).

Table 1. Characteristics of reference conductors.

Conductor Type	Nominal Ampacity [A]	Ambient Temperature [°C]	Irradiance [W/m^2]	Wind Speed [m/s]	Wind Incident Angle [°]	Max. Temperature [°C]
Zebra	636	50	1200	0.6	90	80
Bear	480	50	1200	0.6	90	80
Aster570	702	50	1200	0.6	90	80
Zambeze	1085	35	1200	0.6	90	80
Rail	995	35	1200	0.6	90	80

The first illustrative simulation involves the analysis of the weather conditions on the convective power. For illustrative proposes, considering the reference extreme weather conditions, T_a =40 °C, T_{max} = 80 °C, δ =45°, Irr = 1000 W/m^2, for a Zambeze conductor it is possible to identify in Figure 1 the limit wind speed and angles for the case where the conductor is cooling and heating. Dark red means the conductor is heating while dark blue means it is cooling when compared to the manufacturer's reference conditions.

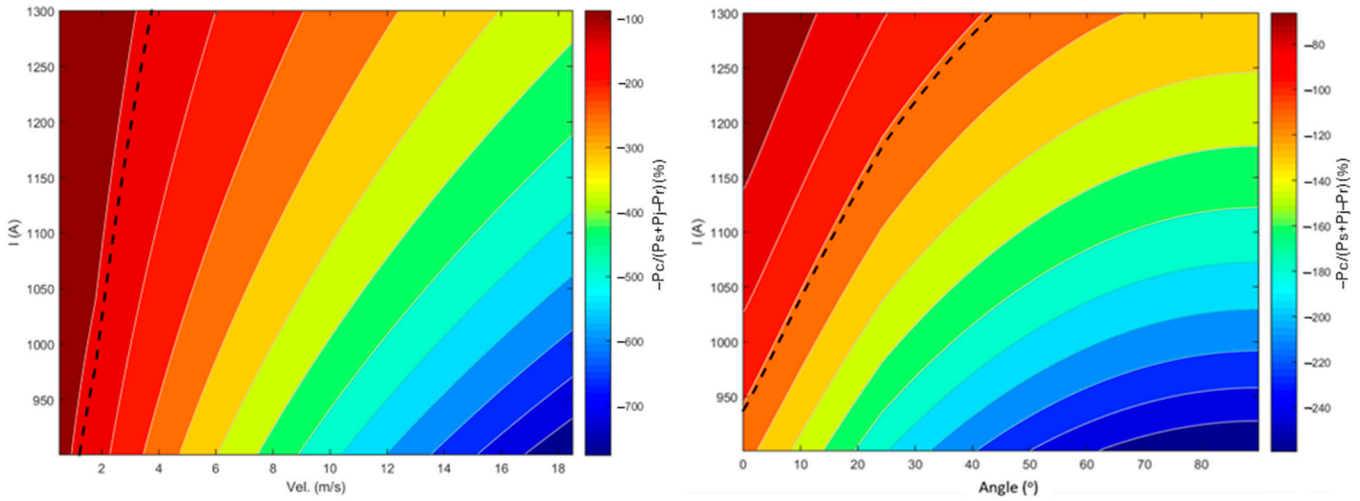

(**a**) (**b**)

Figure 1. Variation of the convective power weight with the current and the (**a**) wind speed and (**b**) incident angle. Dotted lines indicate the limit between heating and cooling values.

Analyzing Figure 1a it is possible to verify that, for the reference conditions and a wind speed of 1.3 m/s, the maximum permanent current that the conductor supports is 900 A, while for a wind speed of 3.8 m/s it supports 1300 A. It is also possible to verify that the increase in wind speed leads to a non-linear relationship between the convective power and all other thermal powers. For the reference conditions the convective power could be approximately equal to all the other thermal powers (when it is −100%) or seven times higher for wind speeds higher than 16 m/s.

For a wind speed of 3.8 m/s, the effect of changing the wind speed incident angle on the relationship between the convective power and the other thermal powers in Figure 1b was analyzed. Analyzing Figure 1b and Equation (6), it is possible to verify that the effects of the incident angle on the relationship between the convective cooling and the other thermal powers are not linear and that the incident angle has a lower importance in relation to the wind speed. In this case the convective power varies from −20% to 250% in relation

to all the other thermal powers. Naturally, with the increase in the wind incident angle the convective power increases, such as the limit ampacity of the conductor. The ambient temperature has a direct effect on the convective and radiative power. So, by using reference variables for a wind speed of 1.3 m/s it is possible to analyze its effect on the convective and radiative powers in Figure 2.

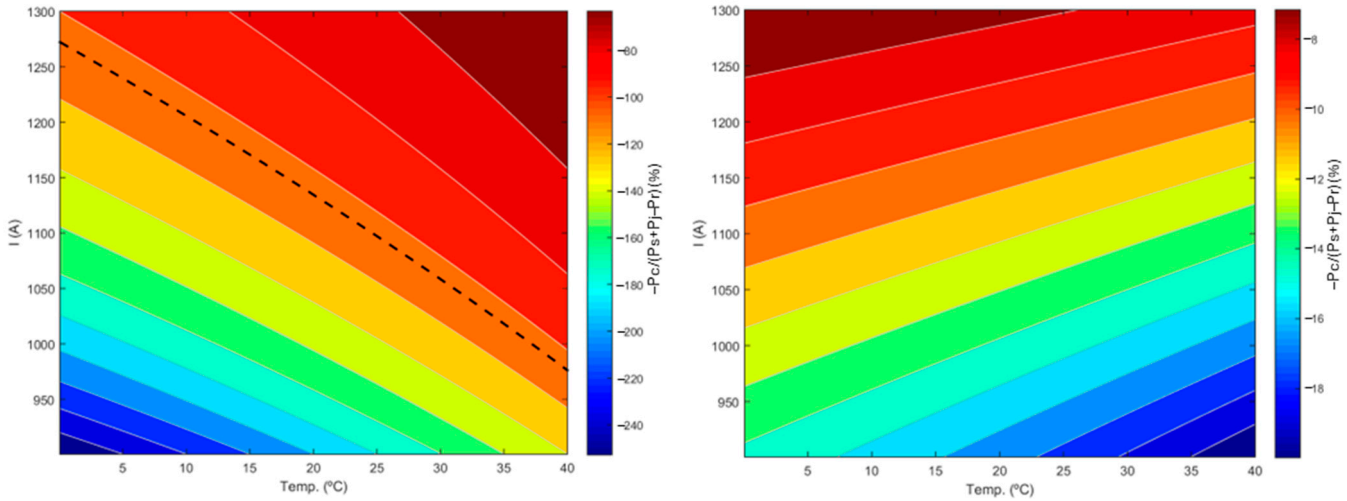

(**a**) (**b**)

Figure 2. Variation of the (**a**) convective and (**b**) radiative power weights with the ambient temperature and the current. Dotted lines indicate the limit between heating and cooling values.

Analyzing Figure 2a it is possible to verify that the higher the ambient temperature the lower the convective cooling with an effect lower than the incident angle. As identified in Equation (5) the ambient temperature has a direct effect over the radiative cooling. The relationship between this power and all other thermal powers can be verified in Figure 2b. Figure 2b shows an increase in the radiative cooling weight when the ambient temperature increases. Normally, radiative cooling has a lower absolute weight in the thermal equilibrium than the convective cooling (see Equation (1)). So, considering Equation (5), the radiative cooling tends to decrease with an increase in the ambient temperature. As in the other figures, this figure illustrates the relationship with the other thermal powers, and as the temperature is also a variable of the convective cooling, in this case it is possible to verify that the negative effect of an increase in the ambient temperature is higher for the convective cooling than the radiative cooling. Figure 3 illustrates the weight of the solar heating in the thermal equilibrium.

Analyzing Figure 3 it is possible to verify that the solar heating has a very small weight in the thermal equilibrium and a linear relation with the irradiance. So, the higher the irradiance the higher the solar heating as can be verified in Equation (4). The goal of the presented work consists in developing a strategy that during real-time operation can rapidly identify the line's critical sector that is used to compute the DLR of the conductor. Considering this goal, it is important to simplify the CIGRÉ formulation without substantially affect outputs. One solution can be pursued by using the thermal powers of a reference scenario to easily identify the critical sector.

Now, considering a Zebra conductor with the following reference values: T_a = 20 °C, T_{max} = 80 °C, v =12 m/s, δ =45°, Irr = 1000 W/m^2, I = 1000 W/m^2, Pc = 100.14 W/m, Pr = 24.97 W/m, Ps = 7.15 W/m, Pj = 72.63 W/m, the reference relation between cooling and heating powers is:

$$Pref = \frac{Pc + Pr}{Ps + Pj} = 1.5682 \quad (24)$$

So, it means that, considering the reference conditions, the conductor is cooling. Accordingly, Figure 4 presents the effect of varying the conductor's ampacity and each one of the weather sensitivity variables concerning the reference power.

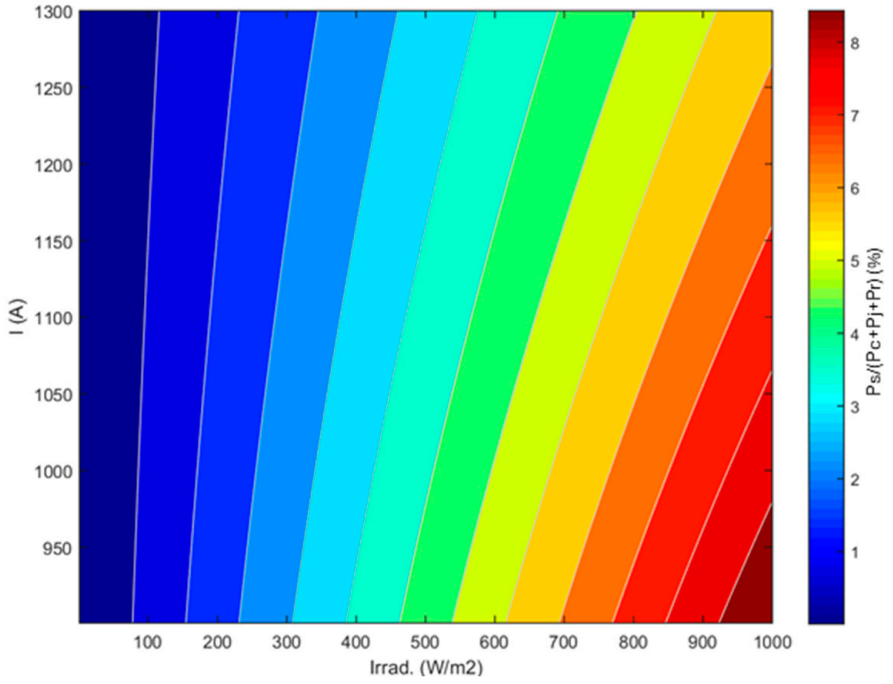

Figure 3. Variation of the solar power weight with the irradiance and the current.

From Figure 4 it is possible to verify the analysis performed before: wind speed is the variable with a higher effect on the DLR computation.

From Figure 4a it is possible to verify that, changing the wind speed from 0 to 25 m/s and the current intensity from 900 to 1100 A, it is possible to detect a change in the reference power from −200% (dark blue, cooling) to 100% (dark red, heating). The same is valid for the incident angle that varies from 0 to 90°. In Figure 4b it is possible to verify that the incident angle is the second most important variable with a variation around −60% and 60% in relation to the reference power.

From Figure 4c,d it is possible to verify the importance of the temperature and the irradiance, easily identifying that these variables have less importance, with their variation in relation to the reference between −50% and 30%. However, for low wind speeds, in the case of natural convection (see Equations (6) and (7)) the cooling convection only depends on the ambient temperature. So, under these circumstances the thermal powers only depend on the temperature and the irradiance.

Figure 5 illustrates the variation of the Nusselt number of the natural and forced convections considering wind speeds between 0.1 and 0.6 m/s and ambient temperatures of 0 °C and 40 °C. The Nusselt number indicates the existence or not of forced convection. The Nusselt number depends on: (i) the incident wind speed on the conductor, (ii) the type of conductor, (iii) the ambient temperature and (iv) the altitude of the conductor above sea level. For a specific conductor, all these parameters are variables except for the type of conductor. Depending on the conductor and on these variables, the Nusselt number is normally neglected for wind speeds below 0.1 m/s, when only natural convection is considered.

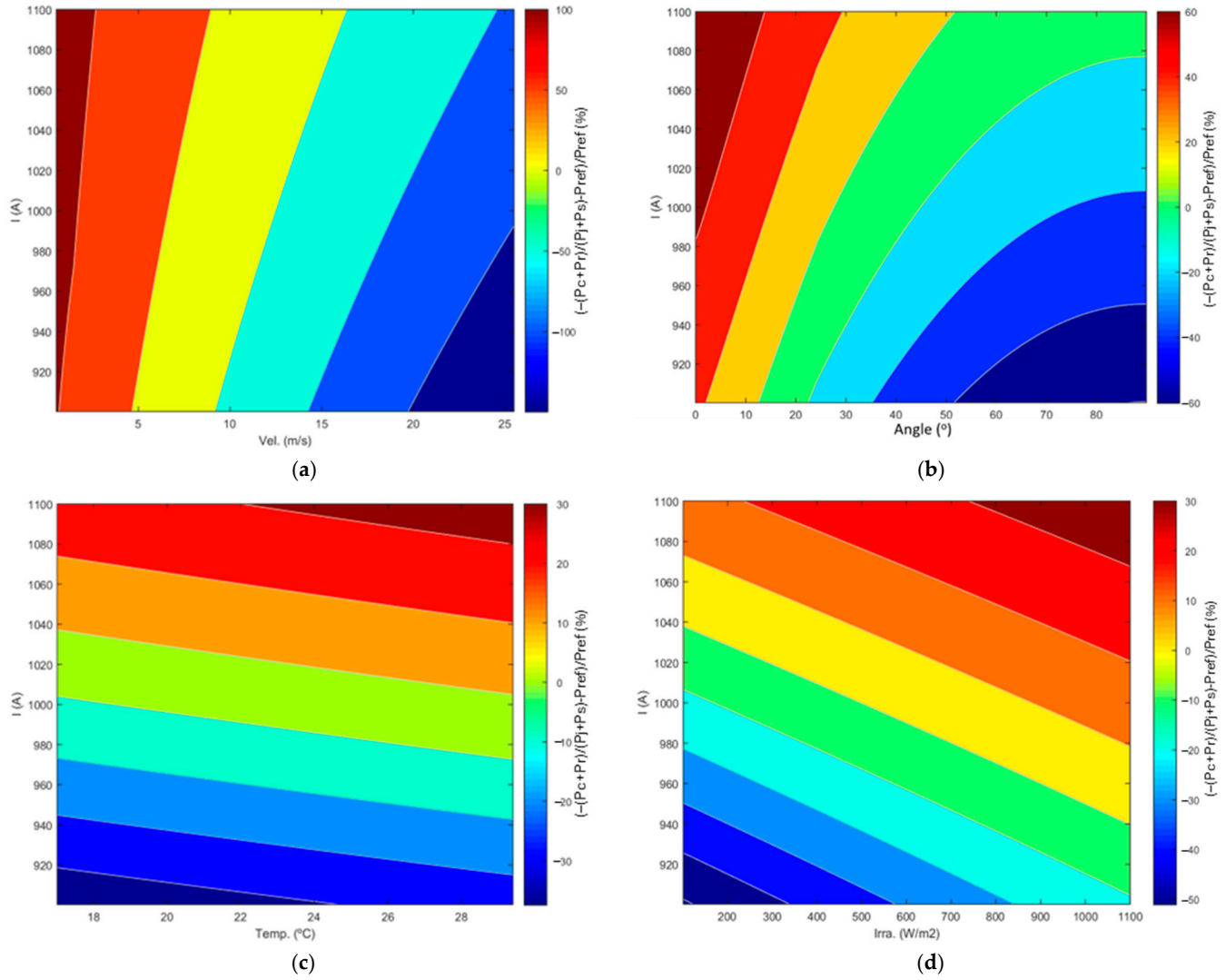

Figure 4. Variation of the thermal powers' weight with the (**a**) wind speed, (**b**) wind angle, (**c**) temperature and (**d**) irradiance.

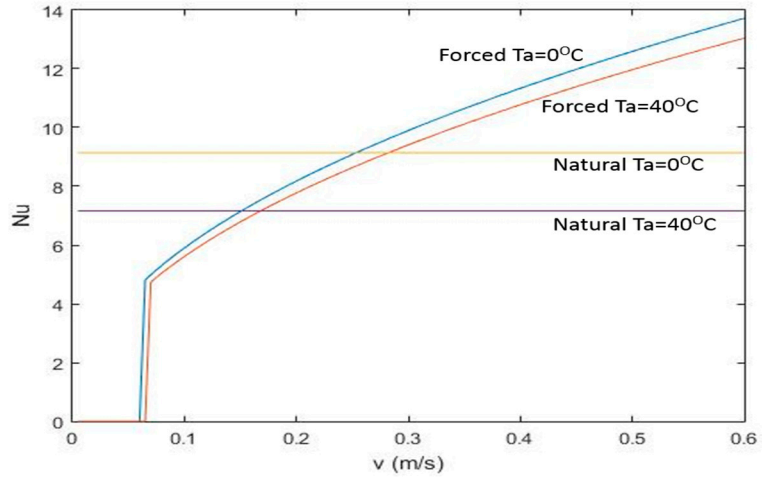

Figure 5. Variation of the Nusselt number considering the natural and forced convections with the wind speed and the ambient temperature.

From Figure 5 it is possible to verify that significant changes in the ambient temperature have a relevant impact on the Nusselt number of the natural convection but a small

impact on the Nusselt number of the forced convection. From Figures 6–8 it is possible to verify that, between 0.1 and 0.5 m/s, the natural and forced convection are selected about the same number of times (see Equation (19)).

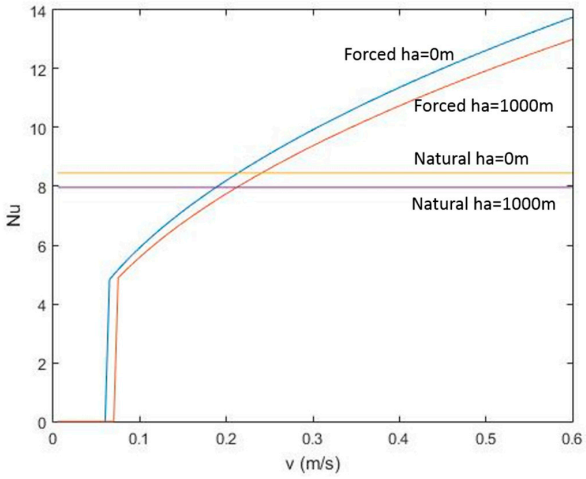

Figure 6. Variation of the Nusselt number considering the natural and forced convections with the wind speed and the conductor altitude.

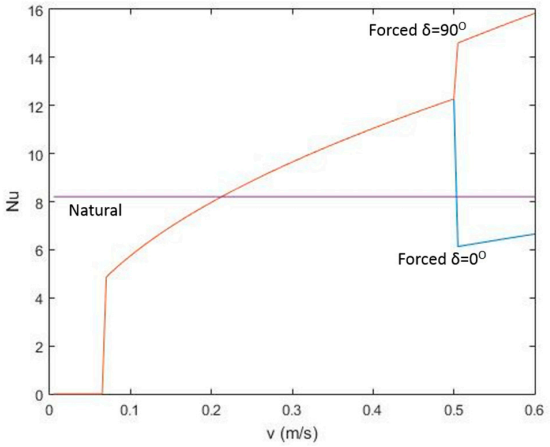

Figure 7. Variation of the Nusselt number considering a natural and forced convection with the wind speed and incident angle.

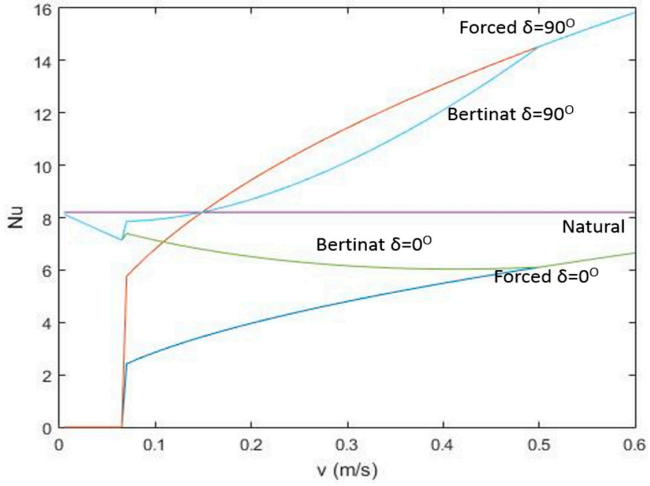

Figure 8. Variation of the Nusselt number with the wind speed and incident angle using the Bertinat formulation.

Figure 6 presents the same study but considering variation in the altitude above sea level of the conductors between 0 and 1000 m. From Figure 6 it is possible to verify that the altitude effect is almost neglected, however, this variable has a higher impact on the forced convection than the natural convection.

Figure 7 illustrates one of the main problems of the CIGRÉ formulation: the lack of continuity between the passages from wind speeds lower than 0.5 m/s to higher wind speeds. From Figure 7 it is possible to verify the existence of a significant change between the Nusselt number used to compute the forced convection when the wind speed is higher than 0.5 m/s. Furthermore, the greater the difference between the incident angle of the wind speed and 45° (fixed for wind speeds until 0.5 m/s) the higher the discontinuity of the computation.

To solve this discontinuity problem, Bertinat presented a methodology where for wind speeds up to 0.5 m/s, the weight of the Nusselt number of the natural and forced convections varies with the wind speed [9]. Figure 8 illustrates the results of the Bertinat methodology, formulated as follows:

$$\mathrm{Nu} = \mathrm{Nu_{NC}} + \frac{\mathrm{v}}{0.5} * (\mathrm{Nu_{FC}} - \mathrm{Nu_{NC}}) \quad (25)$$

From Figure 8 it is possible to identify that, using this methodology, it is possible to have full continuity when passing from wind speeds of 0.5 m/s to higher wind speeds. However, this methodology has errors when computing the Nusselt number up to wind speeds of 0.5 m/s, mainly for small wind incident angles, where the difference between the highest Nusselt number (natural convection) and the Bertinat value is significant. This occurs because this methodology is "following" the forced convection, mainly when wind speeds get closer to 0.5 m/s, neglecting the natural convection.

So, as the wind speed is the most important weather sensitivity variable, the main findings of this section are important to define a methodology to rapidly detect the critical sectors of transmission lines, as illustrated in Table 2.

Table 2. Main conclusions of the theoretical analysis of the CIGRÉ formulation for convective power.

Wind Speed	0.1 m/s	0.1 to 0.5 m/s	0.5 m/s
Background	Natural convection, fixed wind speed and incident angle	Natural or forced convection, fixed incident angles	Forced convection
Conclusions	Only changes in the ambient temperature and in the irradiance indicate the critical sector	The wind speed, the ambient temperature and the irradiance are the variables that indicate the critical sector. High discontinuity when compared with sectors with wind speeds higher than 0.5 m/s	Essentially small changes in the wind speed and direction indicate the critical sector

5. Pre-Solve Methodologies

During real-time operation, distribution and transmission system operators can measure line temperatures to detect congestion when lines approach saturation. However, measurement equipment is installed in only a limited number of sectors per line. To identify the critical sector, real-time weather sensitivity variables can be used to rapidly compute the DLR of the line. For planning purposes and validation of market transactions, TSOs may employ an indirect DLR approach, utilizing the CIGRÉ thermodynamic model for overhead lines. This method relies on weather condition forecasts across different sectors of each line [40]. However, the CIGRÉ formulation is complex and it is not easy to obtain fast outputs in lines with hundreds of sectors. TSOs may employ a pre-solve methodology

to rapidly identify the critical sector of a transmission line by using weather condition forecasts and their effects on thermal ratings, as discussed in the previous section. This approach helps prevent the removal of more competitive bids from energy markets by considering expected rather than static weather conditions. Additionally, weather forecasts and DLR calculations should be continuously updated throughout subsequent market stages, including programmed dispatches, up to real-time operation. The weather conditions across all sectors influence the temperature of the transmission line. However, selecting the critical sector to determine the line's capacity serves as a risk mitigation strategy due to the inherent uncertainties in weather forecasts. During real-time operation, TSOs must decide whether to implement risk mitigation measures to prevent congestion and line saturation. These measures may include triggering re-dispatch, curtailments, balancing reserves and other interventions to ensure the security and stability of the power system.

Figure 9 presents the pre-solve methodology's purpose by using the thermodynamic model shown in Section 3 and the meteorological analysis presented in Section 4.

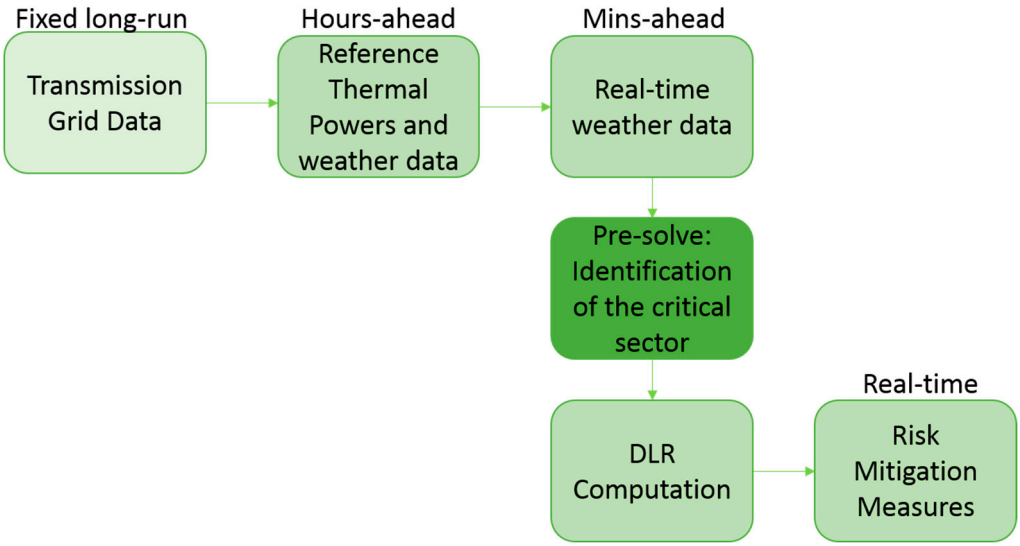

Figure 9. Pre-solve methodology employed to identify the critical sector.

The methodology with the goal of close to real-time operation rapidly identifies the critical sector of each line that defines the DLR of the line. It uses the last reference meteorological data that defined the DLR of the line, such as the computed thermal powers using the CIGRÉ formulation [9].

Then, using real-time meteorological data and the pre-solve method, it is possible to identify the critical sector of the line, rapidly computing the DLR of it (using the complete methodology illustrated in Section 3) instead of hundreds of sectors, minutes ahead of real-time operation.

Thus, performing a regression that relates the weather sensitivity variables to the conductor ampacity and considering Equation (20), the effect of the weather sensitivity variables on the conductors presented in Table 1 can be computed as:

$$f_v = -0.2188v^2 + 19.56v \tag{26}$$

$$f_\delta = -0.0056\delta^2 + 1.0435\delta + 32.78 \tag{27}$$

$$f_{T_a} = -2.01T_a + 167.30 \tag{28}$$

$$f_{Irr} = 0.0143Irr \tag{29}$$

These functions are obtained through a regression analysis performed in Microsoft Excel using more than 10^8 points. In relation to the wind speed regression, this presents some small errors, mainly for wind speeds lower than 0.5 m/s, as can be seen in Figure 10a. It occurs mainly because of the lack of continuity in the DLR model presented in Section 3 (see Equation (19)) and illustrated in Figure 9.

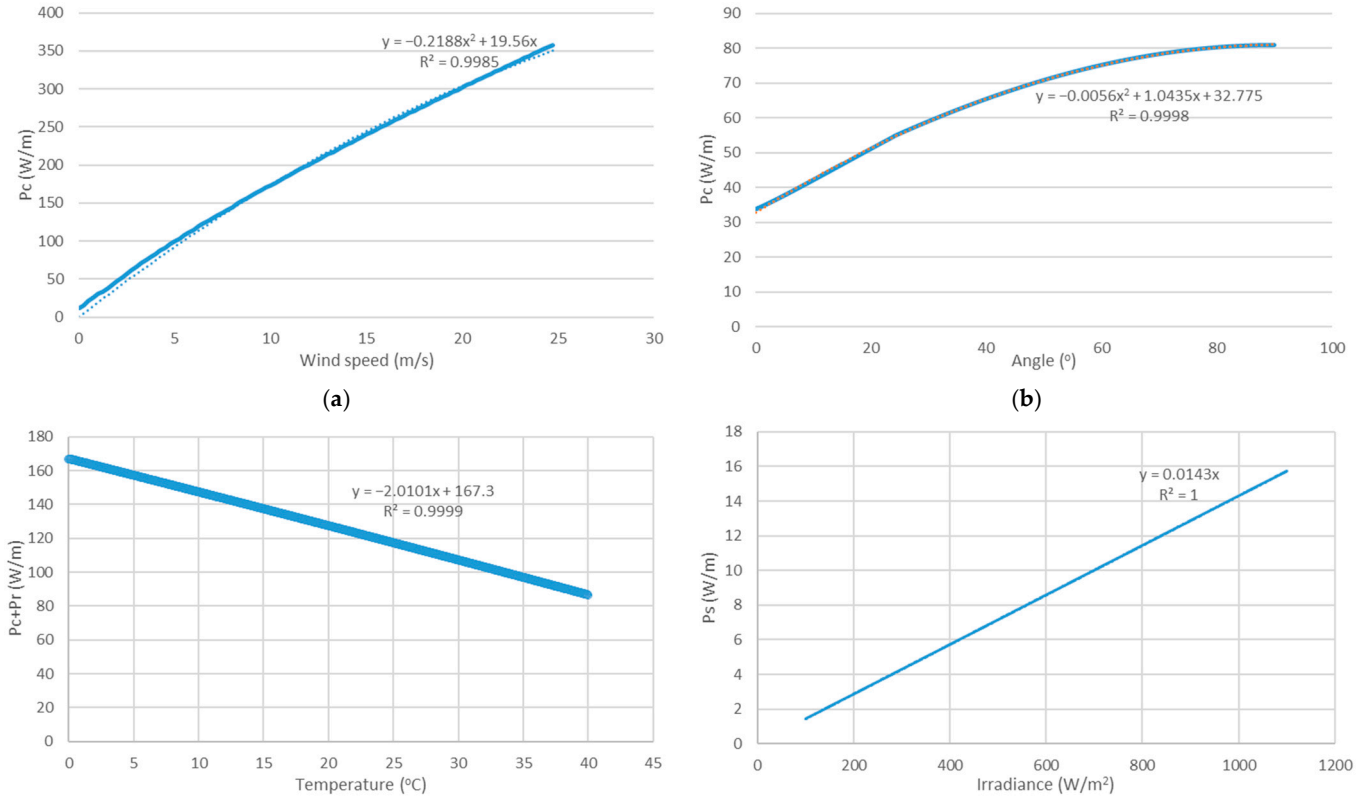

Figure 10. Regression analysis on the effect of (**a**) wind speed, (**b**) wind angle, (**c**) temperature and (**d**) irradiance.

Taking into account the thermodynamic formulation of the conductors to compute the DLR presented in Section 3, the effect of the meteorological conditions presented in Section 4 and the methodology illustrated in Figure 9, the main formulation of the pre-solve analysis to obtain the power variation between the reference case and each sector, s, presented in a specific line, $line_{ij}$, from node i to j in the case of natural convection is presented:

$$\Delta P_s = 2.01\Delta T_{a_s} + 0.0143\Delta Irr_s + 0.2188v_{ref}^2 - 19.56v_{ref} + 0.0056\left(\delta_{ref} - 45\right)^2 - 1.0435\left(\delta_{ref} - 45\right) \; \forall s \in line_{ij} \quad (30)$$

Subject to:

$$\Delta T_{a_s} = T_{a_s} - T_{a_{ref}}, \; \Delta Irr = Irr_s - Irr_{ref}, \; v_s = 0, \; \delta_s = 45^\circ \quad (31)$$

where ΔT_s is the difference between the ambient temperature of the conductor's sector, T_{a_s}, and the reference ambient temperature, $T_{a_{ref}}$. ΔIrr is the difference between the irradiance of sector s, Irr_s, and the reference irradiance, Irr_{ref}.

This conducts to a matrix, $[\Delta P_{ij}]$, with all computed power variations in relation to the reference.

$$[\Delta P_{ij}] = \begin{bmatrix} \Delta P_1 \\ \vdots \\ \Delta P_s \end{bmatrix} \tag{32}$$

Then it is possible to compute the critical sector, C_{ij}, of $line_{ij}$ by considering the minimum value of the matrix:

$$C_{ij} = \min(\Delta P_{ij}) \tag{33}$$

In the case of forced convection, the wind speed and the incident angle are the most important variables but the ambient temperature and the irradiance have also to be considered to obtain the critical sector.

$$\Delta P_s = \begin{matrix} 0.2188\Delta v_s^2 - 19.56\Delta v_s + 0.0056\Delta\delta_s^2 \\ -1.0435\Delta\delta_s + 2.01\Delta T_{a_s} + 0.0143\Delta Irr_s \end{matrix} \quad \forall s \in line_{ij} \tag{34}$$

Subject to:

$$\Delta v = v_s - v_{ref},\ \Delta\delta = \delta_s - \delta_{ref},\ \Delta T_{a_s} = T_{a_s} - T_{a_{ref}},\ \Delta Irr_s = Irr_s - Irr_{ref} \tag{35}$$

where Δv is the difference between the wind speed of sector s, v_s, and the reference wind speed, v_{ref}. $\Delta\delta$ is the difference between the incident angle of sector s, δ_s, and the reference incident angle, δ_{ref}.

In the case of wind speeds between 0.1 and 0.5 m/s the convection can be natural or forced considering the Nusselt number (see Equation (19) and Figure 7), with the wind incident angle constant (45°) and the critical sector computed considering the following formulation in Equation (34):

$$\Delta v = v_s - v_{ref},\ \Delta\delta = \delta_s - 45,\ \Delta Ta_s = T_{a_s} - T_{a_{ref}},\ \Delta Irr_s = Irr_s - Irr_{ref} \tag{36}$$

The first methodology considers all variables using Equation (30) when wind speed is lower than 0.1 m/s and Equation (34) otherwise. The second methodology follows the CIGRÉ brochure as explained in Section 3. For wind speeds up to 0.5 m/s the computation of the Nusselt number could be a solution to reduce the error in the transition to wind speeds higher than 0.5 m/s, but it substantially increases the computational burden of the pre-solve methodology. So, a second methodology is employed to mitigate this issue. The first methodology considers that, for wind speeds below 0.1 m/s, the convection is natural and, on the contrary, it is forced with an incident angle of 45° until 0.5 m/s and variable otherwise. This second methodology only considers that the convection is forced for wind speeds higher than 0.5 m/s. So, between 0.1 and 0.5 m/s it considers the weight of the forced convection, w. So, Equation (35) is subject to the following conditions:

$$\Delta v = v_s - w * v_{ref},\ \Delta\delta = \delta_s - w * \delta_{ref},\ \Delta T_{a_s} = T_{a_s} - Ta_{ref},\ \Delta Irr_s = Irr_s - Irr_{ref} \tag{37}$$

In the previous section it was identified that the forced convection was selected in around 50% of the cases. So, the weight ($w = 0.5$) should reflect those results.

A third methodology considers the outcomes of the Bertinat methodology and computed the weight of the forced convection dynamically considering the wind speed domain between 0.1 m/s,v_{min}, and 0.5 m/s, v_{max}.

$$w = \frac{v_s - v_{min}}{v_{max} - v_{min}} = \frac{v_s - 0.1}{0.5 - 0.1} = \frac{v_s - 0.1}{0.4} \tag{38}$$

Figure 11 illustrates the considerations in all methodologies. As can be seen in Figure 11, differences in the methodologies only occur when the wind speeds range between 0.1 and 0.5 m/s. They occur because the convection can be natural or forced, and the literature does not have a straight formulation to solve the thermodynamic model of the conductor, resulting in errors when adapting a simplified formulation as the pre-solve methodology.

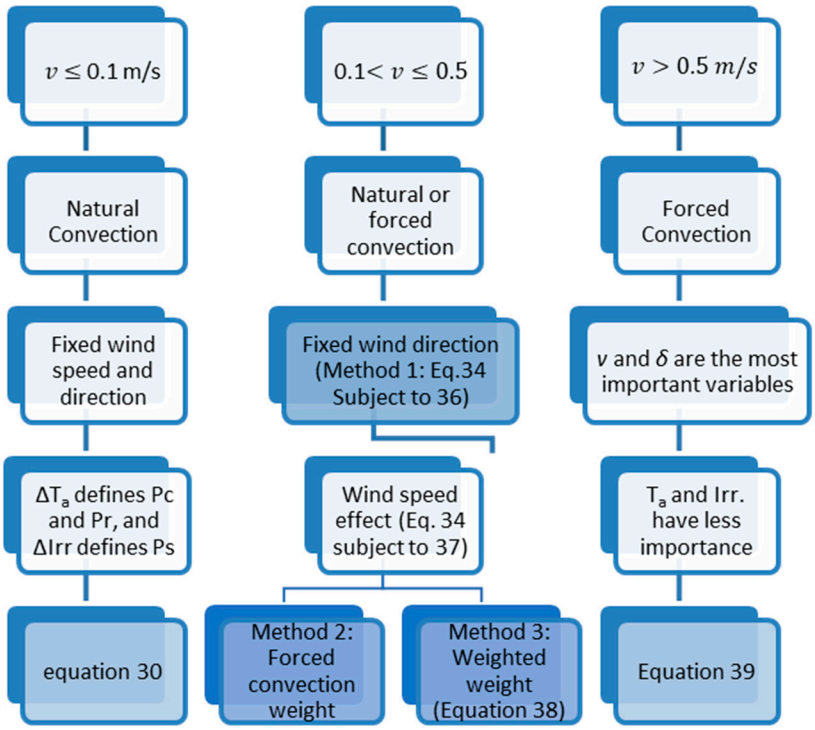

Figure 11. Illustration of the three pre-solve methodologies.

The first methodology is the fastest by not mitigating the thermodynamic discontinuity between 0.1 and 0.5 m/s. The third methodology is the slowest by computing the weight of the forced and natural convection according to the wind speed in Equation (38) when compared to the second methodology that considers a fixed weight besides trying to mitigate the discontinuity of the model.

6. Case Study on the Application of Pre-Solve Methodologies

The numerical weather prediction (NWP) meteorological data are used essentially to obtain precise time series of meteorological parameters that represent a region, without needing the installation of an extensive and expensive network of meteorological stations [15]. This work uses data with a resolution of one hour for the wind speed and direction, temperature and irradiation during the year 2016. The weather parameters necessary in the DLR analysis were derived from an NWP model, with a high spatial resolution (1 km $\times$ 1 km), as described in detail in [15]. The data are from an altitude of 35 m above sea level and collected from some lines used in the case studies presented in this work.

For the regions under analysis, the georeferenced layout and topology of the Portuguese national transmission grid (RNT) considering the identification of all buses/substations and power stations and their electrical characteristics (e.g., conductors, resistance, reactance and susceptance) were obtained from the 2024 RNT annual report [46]. The power grid under study considered the lines of the selected regions operating at 400, 220 and 150 kV. The designed power capacity in each line varies seasonally. As an example, the pre-set meteorological conditions used by the TSO during the winter are wind speed of 0.6 m/s,

radiation of 1000 W/m^2 and an ambient temperature of 15 °C. The different types of electric lines used in this work and their main conductors' characteristics are presented in [13]. The DLR analysis was applied to two different regions in Portugal. The characteristics of each region are provided in the following section.

6.1. Scenarios

Region A has a high penetration of wind power. Given the orographic conditions and resource availability, wind power capacity is mostly located in the mountain regions of central/north Portugal. In the center exists a windy region known as Pinhal Interior where 49 wind parks with a total capacity of 1766 MW and 15 hydropower plants with a total capacity of 1113 MW are installed and operating. This case study was selected to assess the impact of using the pre-solve methodology in a region with a high penetration of wind generation. The region contains 22 high-voltage lines with 1038 sectors. Region B is in the south of Portugal, a region with a high capacity of solar generation considering the orographic conditions and resource availability. The installed PV capacity is approximately 450 MW. A significant short-term increase in the installed PV capacity is expected given the recent public calls for tenders and bilaterally contracted grid access to PV power plants (during 2019) throughout the country. This use of this region will support in assessing the impact of using the pre-solve methodology in a region with very high solar potential and limited grid capacity. The region has 42 high-voltage lines with a total of 1795 sectors (see [13,41] for details).

6.2. Results

This section uses pre-solve methodologies to rapidly identify the critical sector of the lines. However, such methodologies approximate the methodology presented in Section 3, which can lead to errors. One of the most used methodologies to compute the error of regressions is the mean absolute percentage error (MAPE). The error in relation to the real maximum power can be computed as follows:

$$MAPE = \frac{\overline{|S_{PS} - S|}}{S} * 100 = \sum_{l=1}^{L} \frac{\left|S_{PS}^{l} - S^{l}\right|}{S^{l}} / L * 100\ [\%] \tag{39}$$

where S_{PS} is the apparent power (MVA) obtained using a pre-solve methodology and S is the apparent power of the line using the thermodynamic methodology presented in Section 3. L is the number of lines and l is the lines' index. When the pre-solve methodology identifies the real critical sector it attributes to the binary variable b_{cs} the value 0, otherwise its value is 1, with the error in the identification of the critical sector, e_{cs}, being computed using the average value of this variable:

$$e_{cs} = \overline{b_{cs}} * 100\ [\%] \tag{40}$$

The average apparent power difference (MVA), $\overline{\Delta_p}$, from the apparent power obtained using the pre-solve methodology is equal to:

$$\overline{\Delta_p} = \sum_{l=1}^{L} \frac{\left|S_{PS}^{l} - S^{l}\right|}{L} \tag{41}$$

Using the first pre-solve methodology it is possible to compute the DLR of the lines in region A with a MAPE of 1.61%. However, the identification of the critical sectors has an error of 28.6%. This error is substantial because of the high spatial resolution of the meteorological data, causing only small meteorological differences between sectors, which

increases the difficulty to detect the real critical sector. Figure 12 presents the descendent relative and absolute deviations in these regions and Table 3 presents a summary of the main results of the pre-solve methodologies in regions A and B.

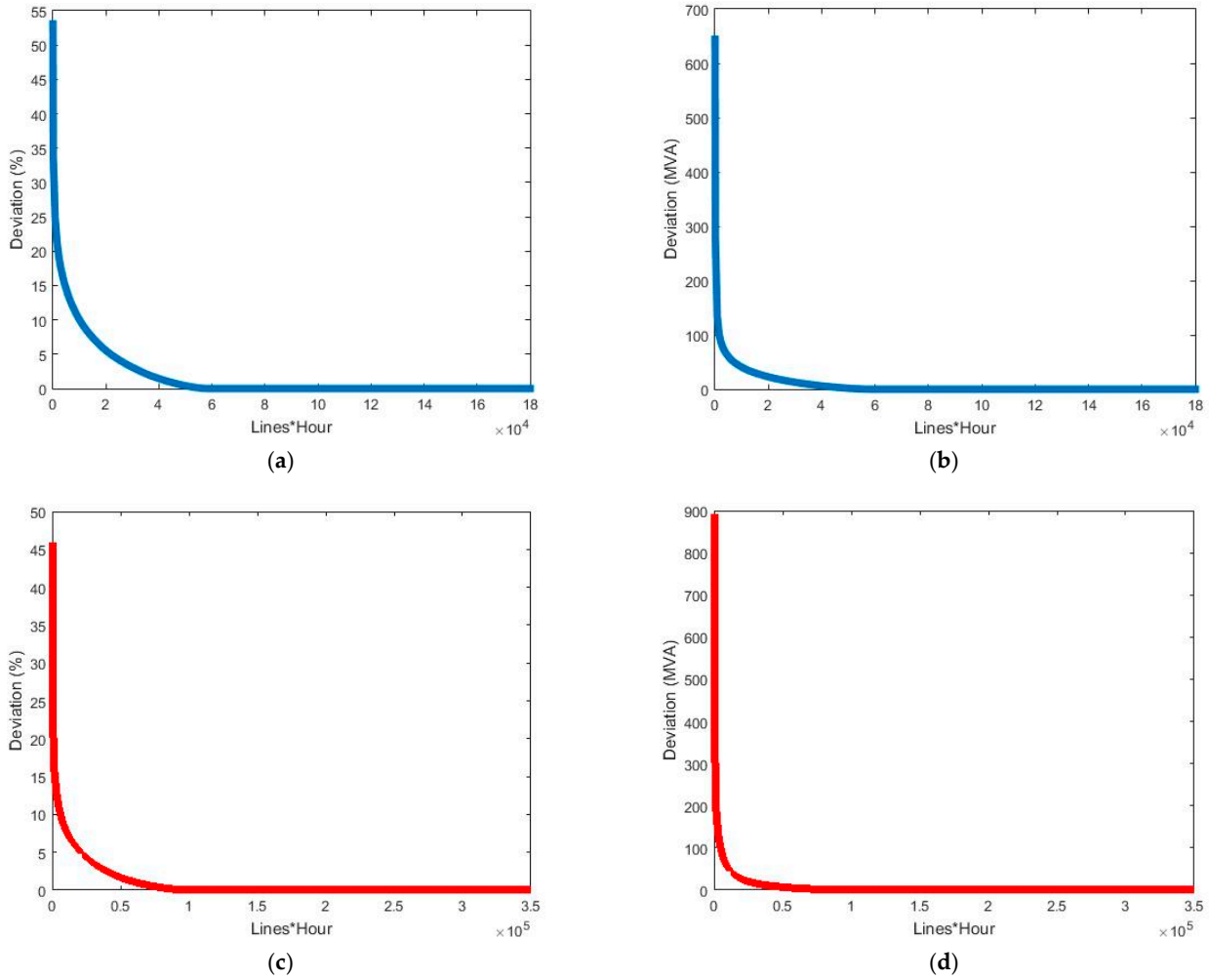

Figure 12. Pre-solve relative (**a**,**c**) and absolute power (**b**,**d**) deviations in relation to the real power in regions A (**a**,**b**) and B (**c**,**d**).

Table 3. Main results of the pre-solve methodologies in regions A and B.

Method	Equation $v \in]0.1;0.5]$	MAPE (%)	Max. Deviation (%)	Average Power Deviation (MVA)	Max. Power Deviation (MVA)
1	34, 36	1.61 (A) 1.24 (B)	53.08 (A) 51.79 (B)	7.13 (A) 7.61 (B)	644 (A) 893 (B)
2	34, 35, 37	0.91 (A) 0.85 (B)	39.73 (A) 45.85 (B)	4.78 (A) 5.76 (B)	644 (A) 893 (B)
3	34, 37, 38	0.86 (A) 0.83 (B)	39.73 (A) 45.85 (B)	4.62 (A) 5.72 (B)	644 (A) 893 (B)

In region A, when extremely hot weather conditions occur, the line limit ampacity is small, with significant deviations (>25%) in less than 0.42% of the cases. Around 5.19% of the cases have deviations higher than 10% and 23% have a deviation higher than 1%. So, in 77% of the cases the deviation between the computed DLR using pre-solve methodologies

and the CIGRÉ model is lower than 1%. In 0.81% of the cases the difference between the critical sector obtained with the pre-solve methodology is higher than 100 MVA in relation to the real critical sector. In 17.47% of the cases the difference is higher than 10 MVA. The average power increase because of the pre-solve errors in the identification of the critical sectors is only 7.13 MVA. However, a maximum deviation of 53% was identified. Significant deviations occur in only 0.01% of the cases and are mainly due to the lack of continuity of the DLR methodology when in the sectors of the same line the wind speed varies around 0.5 m/s (see Figure 7).

In region B, the results are better because the weather conditions of the area where the lines are installed are more stable. The MAPE of the methodology is only 1.24% while the selection of the critical sector has an error of 24.77%. Only 0.27% of the cases have deviations higher than 25%, 3.58% have deviations higher than 10% and 19.7% have deviations higher than 1%. In terms of power, in 1.77% of cases the pre-solve methodology indicated a sector with deviations higher than 100 MVA in relation to the CIGRÉ model. Meanwhile, only 14% of the cases indicate deviations higher than 10 MVA. The average power difference because of the pre-solve errors in the identification of the critical sectors is 7.61 MVA. The most deviations occur when the wind speed stands around 0.5 m/s in the sectors of the same line and the convective power is computed using the maximum of the Nusselt number for wind speeds in the interval]0.1, 0.5] m/s (see Equation (19)) and the Nusselt number of the forced convection otherwise (see Equation (14)). So, the second methodology has the goal of mitigating such errors. Using the second methodology significantly reduces the average errors of the pre-solve methodology. In this methodology a weight of 50% for the forced convection was considered. This weight derives from the theoretical study illustrated in Figures 7–9. Using this methodology, the MAPE decreases by 44% and 33% and the average power difference decreases by 2.35 MVA and 1.85 MVA in regions A and B, respectively. The maximum deviation also reduced by around 25% and 11% in regions A and B, respectively. The maximum power difference remains unchanged since these differences occur in cooling conditions, when wind speeds are substantially higher than 0.5 m/s.

The third methodology is the methodology with better results, but it only brings small benefits in relation to the second methodology. It slightly reduces the MAPE and the average deviation in relation to the second methodology. These last two methodologies reduce the pre-solve errors significantly in relation to the first methodology. Since region A is the region with the worst weather conditions to apply the DLR, i.e., a greater incidence of low wind speeds, the use of methodology 2 or 3 highly improved the results in comparison with the use of these methodologies in region B (see [13] for a more detailed description of the average weather conditions in each region).

7. Conclusions

This work presented pre-solve methodologies to rapidly identify the critical sector of overhead lines close to saturation, using the more detailed CIGRÉ model to compute their dynamic line rating (DLR). These methodologies consider the risk of using forecasted weather conditions by indicating the critical sector that defines the capacity of the line, when all sectors contribute to its DLR. It is a risk mitigation approach that mitigates the risk of overestimated cooling weather conditions. Direct DLR approaches shall be used during real-time operation to measure the lines' temperature, avoiding their degradation and potential outages because of overloads.

The case study used real data from two regions in Portugal, one region with high potential for wind power production, but with more instable meteorological characteristics, and another region with high potential for solar power production, with more stable

meteorological conditions. Results from the study allow the conclusion that the use of a pre-solve methodology is very useful in most weather conditions with average errors below 1%, consisting in an increase around 5.5 MVA in the line capacity in relation to the DLR of the most critical sector. However, in around 0.04% of the cases the use of the pre-solve methodology also changed the real DLR of the line by more than 25%, which can be problematic. This occurs mainly when the wind speed stands around 0.5 m/s in different sectors of the same line and because of the lack of continuity in the CIGRÉ formulation presented in Section 3. Wind speeds up to 0.5 m/s are lower than the reference wind speed that TSOs use to compute the "steady-state" line ampacity. So, these situations are more extreme than the usual considered by TSOs. Accordingly, considering this fact and the pre-solve methodology's results, at an operational level when wind speeds are around 0.5 m/s, TSOs should use the more detailed methodology to compute the DLR. The main limitation of the study is that it only compares outputs with the complete CIGRÉ model. So, it can be concluded that the presented pre-solve methodologies can replicate the CIGRÉ model with small errors, but experimental data are needed to validate them using direct DLR approaches.

For future work, the goal is to analyze the error and risk associated with computed line temperatures using pre-solve methodologies in comparison with onsite measurements, assessing the accuracy and reliability of pre-solve methodologies in real-world conditions.

Funding: The author acknowledges the Fundação para a Ciência e Tecnologia (FCT) for the financial support for this study under the OPTIGRID project (PTDC/EEI-EEE/31711/2017).

Institutional Review Board Statement: Not applicable.

Informed Consent Statement: Not applicable.

Data Availability Statement: The datasets presented in this article are not readily available because of its confidentiality. Requests to access the datasets should be directed to hugo.algarvio@tecnico.ulisboa.pt.

Conflicts of Interest: The author declares no conflicts of interest.

Abbreviations

AC	Alternating current
ACSR	Aluminium conductor steel reinforced
DC	Direct current
DLR	Dynamic line rating
MAPE	Mean absolute percentage error
NWP	Numerical weather prediction
QRF	Quantile regression forest
RES	Renewable energy source
RNT	National transmission grid
SLR	Seasonal line rating
TSO	Transmission system operator
vRES	Variable renewable energy source
Indices	
i,j	Line indices
l	Line number
L	Number of lines
N_{cables}	Number of conductors
Parameters	
α	Temperature coefficient per electrical resistance (1/K)
ε	Conductor emissivity
ξ	Conductor orientation in relation to the east reference (rad)

λ_f	Thermal conductivity of air (W/mK)
σ_b	Stefan–Boltzmann constant (kg s^{-3} K^{-4})
A, B, m, n	Experimental parameters
$alpha$	Solar absorptance
D_{cable}	Conductor diameter (m)
g	Gravity acceleration (m^2/s)
h_a	Altitude (m)
k_j	AC/DC resistance constant
$Kelvin$	Conversion factor
Nu	Nusselt number
R_{AC}	AC resistance of the conductor (Ω)
R_{DC}	DC resistance of the conductor (Ω)
R_{DC20}	DC resistance of the conductor at 20 °C (Ω)
T_{max}	Maximum temperature supported by the conductor (°K)
U	Voltage (V)
y	Air density
Variables	
$\left[\Delta P_{ij}\right]$	Power variations matrix
δ	Incident angle in the conductor (red)
θ	Wind direction (rad)
ϑ_f	Kinematic viscosity of air (m^2/s)
μ_f	Dynamic viscosity of the air (m/s)
C_{ij}	Critical sector
f	Waerther-sensitive variable function
Gr	Grashof number
I_{AC}	AC ampacity (A)
I_{DC}	DC ampacity (A)
Irr	Solar irradiance per square meter (W/m^2)
m	Conductor mass (Kg/m)
Pc	Convective cooling (W/m)
Pj	Joule heating (W/m)
Pr	Radiative cooling (W/m)
Pra	Prandtl number
P_{ref}	Reference relation between cooling and heating powers
Ps	Solar heating (W/m)
Re	Reynolds value
S	Apparent power (MVA)
T_a	Ambient temperature (°K)
T_f	Adjacent temperature to the conductor (°K)
T_{sup}	Conductor's temperature (°K)
v	Wind speed (m/s)
w	Weight of the forced convection

References

1. Karimi, S.; Musilek, P.; Knight, A.M. Dynamic thermal rating of transmission lines: A review. *Renew. Sustain. Energy Rev.* **2018**, *91*, 600–612. [CrossRef]
2. Mínguez, R.; Martínez, R.; Manana, M.; Arroyo, A.; Domingo, R.; Laso, A. Dynamic management in overhead lines: A successful case of reducing restrictions in renewable energy sources integration. *Electr. Power Syst. Res.* **2019**, *173*, 135–142. [CrossRef]
3. Fernandez, E.; Albizu, I.; Bedialauneta, M.; Mazon, A.; Leite, P. Review of dynamic line rating systems for wind power integration. *Renew. Sust. En. Rev.* **2016**, *53*, 80–92. [CrossRef]
4. Arroyo, A.; Castro, P.; Martinez, R.; Manana, M.; Madrazo, A.; Lecuna, R.; Gonzalez, A. Comparison between IEEE and CIGRE Thermal Behaviour Standards and Measured Temperature on a 132-kV Overhead Power Line. *Energies* **2015**, *8*, 13660–13671. [CrossRef]

5. Arantegui, R.; Jäger-Waldau, A. Photovoltaics and wind status in the European Union after the Paris Agreement. *Renew. Sustain. Energy Rev.* **2018**, *81*, 2460–2471. [CrossRef]
6. Algarvio, H.; Lopes, F.; Couto, A.; Santana, J.; Estanqueiro, A. Effects of Regulating the European Internal Market on the integration of Variable Renewable Energy. *WIREs Energy Environ.* **2019**, *8*, e346. [CrossRef]
7. *IEEE Std 738–2023 (Revision of IEEE Std 738–2012)*; IEEE Standard for Calculating the Current-Temperature Relationship of Bare Overhead Conductors. IEEE: Piscataway, NJ, USA, 2023; p. 56.
8. Ministry of Economy/Portuguese Republic. Portaria no 596/2010, Diário da República, 147. 2010. Available online: https://dre.pt/pesquisa/-/search/334076/details/maximized (accessed on 2 April 2025).
9. CIGRÉ. *Guide for Thermal Rating Calculation of Overhead Lines, B.243*; CIGRÉ: Paris, France, 2014; Available online: https://e-cigre.org/publication/601-guide-for-thermal-rating-calculations-of-overhead-lines (accessed on 2 April 2025).
10. Sun, X.; Jin, C. Spatio-temporal weather model-based probabilistic forecasting of dynamic thermal rating for overhead transmission lines. *Int. J. Electr. Power Energy Syst.* **2022**, *134*, 107347. [CrossRef]
11. Uski, S. Estimation method for dynamic line rating potential and economic benefits. *Int. J. Electr. Power Energy Syst.* **2015**, *65*, 76–82. [CrossRef]
12. Mínguez, R.; Martinez, R.; Manana, M.; Cuasante, D.; Garañeda, R. Application of Digital Elevation Models to wind estimation for dynamic line rating. *Int. J. Electr. Power Energy Syst.* **2022**, *134*, 107338. [CrossRef]
13. Couto, A.; Duque, J.; Algarvio, H.; Estanqueiro, A.; Pestana, R.; Esteves, J.; Cao, Y. Impact of the dynamic line rating analysis in regions with high levels of wind and solar PV generation. In Proceedings of the 2020 IEEE PES Innovative Smart Grid Technologies Europe (ISGT-Europe), Delft, The Netherlands, 26–28 October 2020; IEEE: Piscataway, NJ, USA, 2020; pp. 1206–1210.
14. Bhattarai, B.; Gentle, J.P.; McJunkin, T.; Hill, P.J.; Myers, K.S.; Abboud, A.W.; Renwick, R.; Hengst, D. Improvement of Transmission Line Ampacity Utilization by Weather-Based Dynamic Line Rating. *IEEE Trans. Power Deliv.* **2018**, *33*, 1853–1863. [CrossRef]
15. Abboud, A.; Gentle, G.; McJunkin, J.; Hill, P.; Myers, K.; Abboud, A. Coupling computational fluid dynamics with the high resolution rapid refresh model for forecasting dynamic line ratings. *Electr. Power Syst. Res.* **2019**, *170*, 326–337. [CrossRef]
16. Teng, F.; Dupin, R.; Michiorri, A.; Kariniotakis, G.; Chen, Y.; Strbac, G. Understanding the benefits of dynamic line rating under multiple sources of uncertainty. *IEEE Trans. Power Syst.* **2017**, *33*, 3306–3314. [CrossRef]
17. Bolgaryn, R.; Wiemer, J.; Scheidler, A.; Braun, M. Security-constrained active power curtailment considering line temperature and thermal inertia. *IET Gener. Transm. Distrib.* **2023**, *17*, 5183–5197. [CrossRef]
18. Maksić, M.; Djurica, V.; Souvent, A.; Slak, J.; Depolli, M.; Kosec, G. Cooling of overhead power lines due to the natural convection. *Int. J. Electr. Power Energy Syst.* **2019**, *113*, 333–343. [CrossRef]
19. Kollenda, K.; Schrief, A.; Biele, C.; Lindner, M.; Sundorf, N.; Hoffrichter, A.; Roehder, A.; Moser, A.; Rehtanz, C. Curative measures identification in congestion management exploiting temporary admissible thermal loading of overhead lines. *IET Gener. Transm. Distrib.* **2022**, *16*, 3171–3183. [CrossRef]
20. Schurig, O.; Frick, C. Heating and current-carrying capacity of conductors for outdoor service. *Gen Electr Rev* **1930**, *33*, 141–157.
21. *EN 50182:2002*; Conductors for Overhead Lines. Round Wire Concentric Lay Stranded Conductors. B S I Standards: London, UK, 2002.
22. International Electrotechnical Commission. *Technical Committee 20—Overhead Electrical Conductors*; International Electrotechnical Commission: Geneva, Switzerland, 2016.
23. Pavlinić, A.; Komen, V. Calculation and analysis of the steady-state line ampacity weather sensitivity coefficients. *Electr. Power Syst. Res.* **2020**, *181*, 106181. [CrossRef]
24. Kirschen, D.; Strbac, G. *Fundamentals of Power System Economics*; Wiley: Chichester, UK, 2018.
25. Sun, B.; Wang, F.; Xie, J.; Sun, X. Electricity Retailer Trading Portfolio Optimization Considering Risk Assessment in Chinese Electricity Market. *Electr. Power Syst. Res.* **2021**, *190*, 106833. [CrossRef]
26. Ardila, L.; Cardona, C. Structure and current state of the wholesale electricity markets. *IEEE Lat. Am. Trans.* **2017**, *15*, 669–674. [CrossRef]
27. Algarvio, H.; Lopes, F.; Couto, A.; Estanqueiro, A.; Santana, J. Variable Renewable Energy and Market Design: New Products and a Real-World Study. *Energies* **2019**, *12*, 4576. [CrossRef]
28. Petitet, M.; Perrot, M.; Mathieu, S.; Ernst, D.; Phulpin, Y. Impact of gate closure time on the efficiency of power systems balancing. *Energy Policy* **2019**, *129*, 562–573. [CrossRef]
29. Sleisz, Á.; Sőrés, P.; Raisz, D. Algorithmic properties of the all-European day-ahead electricity market. In Proceedings of the 11th International Conference on the European Energy Market (EEM 14), Krakow, Poland, 28–30 May 2014; IEEE: Piscataway, NJ, USA, 2014; pp. 1–6.
30. Algarvio, H.; Lopes, F.; Couto, A.; Estanqueiro, A. Participation of wind power producers in day-ahead and balancing markets: An overview and a simulation-based study. *Wiley Interdiscip. Rev. Energy Environ.* **2019**, *8*, e343. [CrossRef]
31. Algarvio, H.; Couto, A.; Duque, J.; Estanqueiro, A.; Pestana, R.; Esteves, J.; Yang, C. Increase cross-border capacity to reduce market splitting of day-ahead electricity markets-A dynamic line rating approach. In Proceedings of the 2022 IEEE/PES

Transmission and Distribution Conference and Exposition (T&D), New Orleans, LA, USA, 25–28 April 2022; IEEE: Piscataway, NJ, USA, 2014; pp. 1–5.
32. Davison, P.; Lyons, P.; Taylor, P. Temperature sensitive load modelling for dynamic thermal ratings in distribution network overhead lines. *Int. J. Electr. Power Energy Syst.* **2019**, *112*, 1–11. [CrossRef]
33. Li, Y.; Wang, Y.; Chen, Q. Study on the impacts of meteorological factors on distributed photovoltaic accommodation considering dynamic line parameters. *Appl. Energy* **2020**, *259*, 114–133. [CrossRef]
34. Viafora, N.; Delikaraoglou, S.; Pinson, P.; Holbøll, J. Chance-constrained optimal power flow with non-parametric probability distributions of dynamic line ratings. *Int. J. Electr. Power Energy Syst.* **2020**, *114*, 105389. [CrossRef]
35. Dupin, R.; Kariniotakis, G.; Michiorri, A. Overhead lines Dynamic Line rating based on probabilistic day-ahead forecasting and risk assessment. *Int. J. Electr. Power Energy Syst.* **2019**, *110*, 565578. [CrossRef]
36. Dupin, R.; Michiorri, A.; Kariniotakis, G. Optimal dynamic line rating forecasts selection based on ampacity probabilistic forecasting and network operators' risk aversion. *IEEE Trans. Power Syst.* **2019**, *34*, 283645. [CrossRef]
37. Yan, Z.; Wang, Y.; Liang, L. Analysis on Ampacity of Overhead Transmission Lines Being Operated. *J. Inf. Process. Syst.* **2017**, *13*, 1358–1371. [CrossRef]
38. Couto, A.; Costa, P.; Rodrigues, L.; Lopes, V.; Estanqueiro, A. Impact of weather regimes on the wind power ramp forecast in Portugal. *IEEE Trans. Sustain. Energy* **2014**, *6*, 934–942. [CrossRef]
39. Zhang, X.; Ying, Z.; Chen, Y.; Chen, X. A thermal model for calculating axial temperature distribution of overhead conductor under laboratory conditions. *Electr. Power Syst. Res.* **2019**, *166*, 223–231. [CrossRef]
40. Michiorri, A.; Nguyen, H.-M.; Alessandrini, S.; Bremnes, J.B.; Dierer, S.; Ferrero, N.; Nygaard, B.-E.; Pinson, P.; Thomaidis, N.; Uski, S. Forecasting for dynamic line rating. *Renew. Sustain. Energy Rev.* **2015**, *52*, 1713–1730. [CrossRef]
41. Estanqueiro, A.; Algarvio, H.; Couto, A.; Michiorri, A.; Salas, S.; Pudjianto, D.; Hägglund, P.; Dobschinski, J.; Bolgaryn, R.; Kanefendt, T.; et al. Dynamic line rating models and their potential for a cost-effective transition to carbon-neutral power systems. *WIREs Energy Environ.* **2025**, *14*, e70002. [CrossRef]
42. Stephen, R.; Douglas, D.; Gaudry, M.; Argasinska, H.; Bakic, K.; Hoffman, S.; Iglesias, J.; Jakl, F.; Katoh, J.; Kikuta, T.; et al. *Thermal Behaviour of Overhead Conductors*; CIGRÉ: Paris, France, 2002.
43. Bergman, T.; Incropera, F.; DeWitt, D.; Lavine, A. *Fundamentals of Heat and Mass Transfer*, 7th ed.; John Wiley & Sons: Hoboken, NJ, USA, 2011.
44. Petela, R. *Engineering Thermodynamics of Thermal Radiation for Solar Power Utilization*; McGraw Hill: New York, NY, USA, 2010.
45. Price, C.; Gibbon, R. Statistical approach to thermal rating of overhead lines for power transmission and distribution. *IEE Proc. C (Gener. Transm. Distrib.)* **1983**, *130*, 245–256. [CrossRef]
46. REN. Caracterização da Rede Nacional de Transporte para Efeitos de Acesso à Rede. 2025. Available online: https://mercado.ren.pt/PT/Electr/AcessoRedes/AcessoRNT/CaractRNT/BibRelAno/Caracteriza%C3%A7%C3%A3o%20da%20RNT%2031-12-2024.pdf (accessed on 2 April 2025).